PERGAMON

Water Research 36 (2002) 3911–3918

WATER RESEARCH

www.elsevier.com/locate/watres

Research note

Dissolution of a well-defined trichloroethylene pool in saturated porous media: experimental results and model simulations

Kenneth Y. Lee[a,*], Constantinos V. Chrysikopoulos[b]

[a] *Department of Civil and Environmental Engineering, Rutgers, The State University of New Jersey, Piscataway, NJ 08854, USA*
[b] *Department of Civil and Environmental Engineering, University of California, Irvine, CA 92697, USA*

Abstract

An experimental mass transfer correlation was developed for trichloroethylene (TCE) pools dissolving in water-saturated porous media. A three-dimensional, bench-scale model aquifer previously designed by Chrysikopoulos et al. (Water Resour. Res. 36(7) (2000) 1687) was employed for collection of the experimental dissolution data. The unique aspect of the model aquifer design is the formation of a well-defined, circular TCE pool at the bottom of the model aquifer. Steady-state dissolved TCE concentrations at specific downstream locations within the aquifer were collected for each of the seven interstitial velocities considered in this study. For each interstitial velocity, a corresponding time invariant overall mass transfer coefficient was determined by fitting the experimental data to an analytical solution applicable to nonaqueous phase liquid (NAPL) pools (Water Resour. Res. 31(4) (1995) 1137). Subsequently, a correlation relating the time invariant overall Sherwood number to appropriate overall Peclet numbers was developed. Relatively good agreement between the newly developed correlation and experimental data was observed.

Keywords: Groundwater; NAPL pool; Dissolution; Contaminant transport; Mass transfer correlation

1. Introduction

The study of nonaqueous phase liquid (NAPL) pool dissolution in saturated porous media has captured the attention of numerous hydrogeologists and environmental engineers over the last decade (e.g., [1–9]). The majority of the NAPL pool dissolution studies available in the literature are focused on theoretical and computational aspects. Only a handful of publications describe experimental investigations conducted in two-dimensional (e.g., [10–13]) and three-dimensional [14] bench-scale model aquifers. Consequently, the existing experimental data sets for NAPL pool dissolution in three-dimensional porous media are not sufficient for development of reliable mass transfer correlations. The only available mass transfer correlations applicable to NAPL pool dissolution in three-dimensional, water saturated porous media are based on numerically generated data [15].

The present work is focused on the development of an experimental mass transfer correlation for circular trichloroethylene (TCE) pools dissolving in three-dimensional, water-saturated porous media. To our knowledge, such correlation has not been published in the literature yet. The experimental work reported by [14] is extended in order to obtain a complete data set of mass transfer coefficients for trichloroethylene (TCE) pool dissolution in a water saturated, three-dimensional bench-scale model aquifer. The unique experimental design employed here allows for the formation of a well-defined, circular TCE pool. Steady-state aqueous phase TCE concentrations were measured at several sampling locations downstream of the pool under various interstitial flow velocities. An overall mass transfer coefficient was obtained for each flow condition by fitting the

*Corresponding author. Tel.: +1-732-445-2240.
E-mail address: kenlee@rci.rutgers.edu (K.Y. Lee).

0043-1354/02/$ - see front matter
PII: S0043-1354(02)00097-0

observed concentrations to an analytical solution derived by [16]. Although analytical solutions of contaminant transport originating from dissolving NAPL pools with elliptic, circular as well as rectangular shape are available in the literature [16], the experimental study presented here focuses only on a circular source, because a pool with approximately circular shape is more likely to form in relatively homogeneous subsurface formations. An experimental power-law expression relating the overall Sherwood number to the appropriate overall Peclet numbers was developed. Furthermore, the proposed relationship was compared to a numerically determined correlation presented by [15].

2. Background

As a NAPL pool dissolves into the interstitial liquid of a water saturated porous formation, a concentration boundary layer is assumed to be developed above the pool–water interface. Assuming that the thickness of the pool is insignificant relative to the thickness of the aquifer, the mass transfer from the pool–water interface to the interstitial liquid is described by the following relationship [16]:

$$-\mathscr{D}_e \frac{\partial C(t,x,y,0)}{\partial z} = k(t,x,y)[C_s - C(t,x,y,\infty)], \qquad (1)$$

where $C(t,x,y,z)$ is the liquid phase solute concentration [M/L^3]; x, y, z are the spatial coordinates in the longitudinal, lateral, and vertical directions, respectively [L]; t is time [t]; $k(t,x,y)$ is the local mass transfer coefficient dependent on time and location at the NAPL–water interface [L/t]; C_s is the aqueous saturation or solubility concentration [M/L^3]; $C(t,x,y,\infty) = C_b = 0$ is the concentration above the concentration boundary layer or background concentration [M/L^3]; and $\mathscr{D}_e = \mathscr{D}/\tau^*$ is the effective molecular diffusion coefficient [L^2/t] (where $\mathscr{D}$ is the molecular diffusion coefficient [L^2/t] and $\tau^* > 1$ is the tortuosity coefficient [dimensionless]).

The concentration within the boundary layer varies from the saturation concentration (C_s) at the interface to the constant background concentration (C_b) in the bulk interstitial fluid. The thickness of the boundary layer depends mainly on the hydrodynamic and dispersive properties of the system, and is defined as the value of z for which $[C_s - C(t,x,y,z)]/[C_s - C_b] = 0.99$ [17, p. 321]. A thin boundary layer represents steep concentration gradients. It should be noted, however, that the greater the concentration gradient the greater the mass transfer from the pool. The local mass transfer coefficient decreases with distance from the front end of the NAPL pool [18].

The local mass transfer coefficient is usually not an easy parameter to determine with precision. Thus, in mathematical modeling of contaminant transport from NAPL pool dissolution, $k(t,x,y)$ is often replaced by the average mass transfer coefficient, $\bar{k}(t)$, for the entire pool expressed as [17]

$$\bar{k}(t) = \frac{1}{A}\int_A k(t,x,y)\,\mathrm{d}^2\mathbf{A}, \qquad (2)$$

where A is the surface area of the NAPL pool [L^2], and $\mathrm{d}^2\mathbf{A}$ is a differential surface area. It should be noted that (2) is valid for the present study because the pool–water interfacial area remains constant over time. At steady-state physicochemical and hydrodynamic conditions the local mass transfer coefficient is independent of time. In this work, it is assumed that steady-state conditions exist and that the average mass transfer coefficient is equal to the time invariant mass transfer coefficient

$$k^* = \bar{k}(t). \qquad (3)$$

Numerous empirical mass transfer correlations have been presented in the literature for residual NAPLs in one-dimensional packed columns [19]. These correlations consist of a leading coefficient and power-law forms of the dimensionless parameters used, and were developed mainly for steady-state flow conditions. Furthermore, mass transfer correlations for rectangular, elliptic and circular NAPL pool shapes in three-dimensional, homogeneous, water saturated porous formations have also been established [15,20]. These correlations are based on numerical simulations. The correlations for circular NAPL pools relate the dimensionless, time invariant overall Sherwood number, $Sh^* = k^*\pi^{1/2}r/\mathscr{D}_e$, to the overall Peclet numbers in x and y directions, $Pe_x^* = U_x r/D_x$ and $Pe_y^* = U_x r/D_y$, respectively, where $D_x = \alpha_L U_x + \mathscr{D}_e$ and $D_y = \alpha_T U_x + \mathscr{D}_e$ are the longitudinal and transverse hydrodynamic dispersion coefficients, respectively [L^2/t] (where α_L and α_T are the longitudinal and transverse aquifer dispersivities, respectively [L]); U_x is the average interstitial velocity [L/t]; and r is the pool radius [L].

For an elliptic/circular NAPL pool in a three-dimensional porous medium the appropriate correlation developed by [15] is given by

$$Sh^* = 1.74(Pe_x^*)^{0.33}(Pe_y^*)^{0.40}. \qquad (4)$$

It should be noted that mass transfer correlations based on numerically generated data, although extremely useful due to their wide range of applicability, are not as reliable as those obtained from experimental observations.

3. Experimental setup

A schematic diagram of the three-dimensional, bench-scale model aquifer used in this study and a blowup of the sampling plate is shown in Fig. 1. It should be noted that all the experimental details are presented by [14]. The model aquifer is constructed by glass with a specially designed aluminum bottom plate. A 0.5 cm deep, circular disk with 7.6 cm diameter is removed from the aluminum sheet in order to form the experimental pool. Glass beads are placed in the pool in order to support a #60 stainless-steel mesh that prevents settling of sand into the pool. A 16 gauge stainless tube inserted into the pool through a horizontal hole drilled along the aluminum sheet is used to deliver the NAPL into the experimental pool. The aquifer material is kiln-dried Monterey sand (RMC Lonestar, Monterey, CA) and the aqueous phase pumped through the experimental aquifer is degassed, deionized water with sodium azide. It should be noted that a total of seven needles are vertically inserted into the aquifer and their locations are indicated on the sampling plate as filled circles. The designation of each sampling port is specified in Fig. 1 by a lower right number; whereas, the needle placement depth, measured in centimeters from the bottom of the aquifer, is indicated by a bold number at the upper left side of each sampling port. The bench-scale model aquifer was placed inside a constant temperature chamber (Forma Scientific, Marietta, OH) maintained at 20°C.

The characteristics of the experimental aquifer are obtained from the work by [14]. The dry bulk density of the sand $\rho_b = 1.61$ kg/L, and the aquifer porosity $\theta = 0.415$ were evaluated by gravimetric procedures. The dimensionless retardation factor, $R = 1.31$, of the aqueous-phase TCE was determined from a column flowthrough experiment. The tortuosity coefficient for the aquifer sand was considered to be $\tau^* = 1.43$ [21]. The molecular diffusion coefficient for the aqueous-phase TCE is $\mathscr{D} = 0.0303$ cm^2/h [22]. The pool radius is $r = 3.8$ cm. Bromide ion in the form of the moderately soluble potassium bromide salt was the tracer of choice [23] for the tracer experiment conducted in order to determine the longitudinal and transverse aquifer

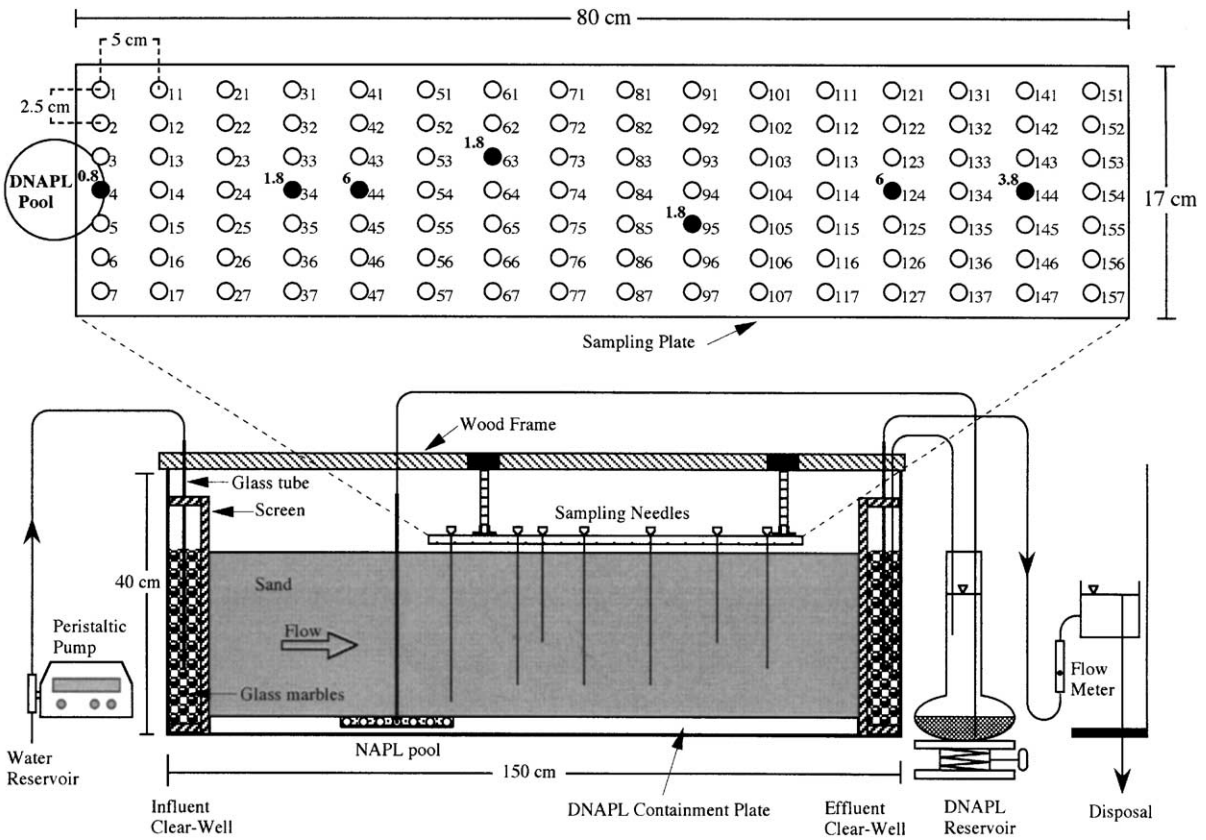

Fig. 1. Schematic diagram of the experimental aquifer and the sampling plate. Filled circles on the sampling plate represent needle placement locations. For each filled circle, the lower right number indicates the sampling port number and the upper left bold numbers indicate the needle placement depth measured in cm from the bottom of the aquifer.

dispersivities $\alpha_L = 0.259$ cm and $\alpha_T = 0.019$ cm, respectively. The experimental pool contained approximately 12 mL of certified ACS grade (Fisher Scientific) TCE with solubility of $C_s = 1100$ mg/L [24]. It should be noted that the biological inhibitor sodium azide was added to the aqueous solution to prevent any possible degradation of TCE and fouling of the system [14]. Consequently, at steady-state conditions the retardation factor has no effect on the concentration distributions of a nondecaying solute within a homogeneous aquifer [11].

4. TCE dissolution data

Following the experimental procedures outlined by [14], four additional TCE dissolution experiments were conducted in the three-dimensional, bench scale model aquifer with interstitial velocities of $U_x =$ 0.51, 1.21, 1.50, and 3.35 cm/h. The interstitial velocity in the aquifer was altered by changing the water volumetric flow rate of the peristaltic pump. Aqueous phase TCE concentrations were collected only when steady-state concentrations were observed at sampling port 144, which is the sampling port farthest away from the TCE pool (see Fig. 1). Note that the cumulative dissolution period for all seven experiments is 2092 h.

For each TCE dissolution experiment, two sets of aqueous samples were collected at two different times (see Table 1) from sampling ports 4 (located at $x = 0.0$, $y = 0.0$, $z = 0.8$ cm), 34 (15.0, 0.0, 1.8), 63 (30.0, 2.5, 1.8), 95 (45.0, −2.5, 1.8), and 144 (70.0, 0.0, 3.8). It should be noted that the origin of the Cartesian coordinate (0, 0, 0) used in this study is directly below port 4. The aqueous samples were collected and analyzed using a gas chromatograph according to the analytical procedure described in [14]. Each aqueous sample was analyzed twice. Although no significant variation in the two measurements was noted, the average of the observed concentrations is presented in Table 1. For completeness, experiments with interstitial velocities $U_x = 0.25$, 0.75, and 1.96 cm/h, previously presented by [14], are also included in Table 1. Furthermore, for each interstitial velocity used the average of the two different aqueous phase TCE concentrations listed in Table 1 are plotted in Fig. 2. A different symbol is used for TCE concentrations observed at each different sampling port. It is evident from Fig. 2 that aqueous-phase TCE concentrations decrease with increasing U_x. For each U_x considered, the highest dissolved concentration is observed at sampling port 4, which is closest to the TCE pool, and the lowest dissolved concentration is observed at node 144, which is the farthest away from the pool. It should be noted that it was assumed here that any possible density variations would not significantly affect the transport of dissolved TCE. It should also be noted that the trend of the TCE concentration data in Fig. 2 is expected because the concentration boundary layer decreases with increasing interstitial velocity [18].

5. Experimental mass transfer correlation

For each set of aqueous-phase TCE concentrations collected, the corresponding k^* is estimated by fitting the

Table 1
Observed aqueous-phase TCE concentrations (mg/L) and estimated k^* values

U_x (cm/h)	Experiment	Time[b] (h)	Sampling node[a]					k^* (cm/h)
			4	34	63	95	144	
0.25	3[c]	720	627.0	206.1	154.9	141.4	71.8	0.0268±0.002
		888	629.2	202.4	148.5	141.1	70.3	0.0267±0.002
0.51	5	336	675.1	154.6	113.4	96.5	56.5	0.0356±0.009
		384	407.3	136.1	114.7	98.2	56.9	0.0332±0.002
0.75	1[c]	237	417.5	117.6	82.2	143.5	43.0	0.0381±0.004
		264	390.0	91.3	78.7	145.8	44.2	0.0378±0.004
1.21	7	168	378.5	134.5	92.4	105.9	24.1	0.0437±0.006
		192	386.3	136.7	97.3	110.8	24.5	0.0438±0.006
1.50	4	121	362.9	121.8	65.4	99.1	37.5	0.0456±0.006
		142	368.1	106.9	59.7	104.1	37.8	0.0456±0.007
1.96	2[c]	120	233.4	77.4	54.5	51.3	17.4	0.0473±0.003
		144	240.5	86.7	54.9	51.2	17.9	0.0474±0.003
3.35	6	54	204.6	69.0	46.8	34.2	4.5	0.0512±0.004
		78	213.3	71.7	42.4	46.0	5.0	0.0513±0.004

[a] The exact locations of the sampling nodes are given in Fig. 1.
[b] The time given is since the initiation of each individual experiment.
[c] Adopted from [14].

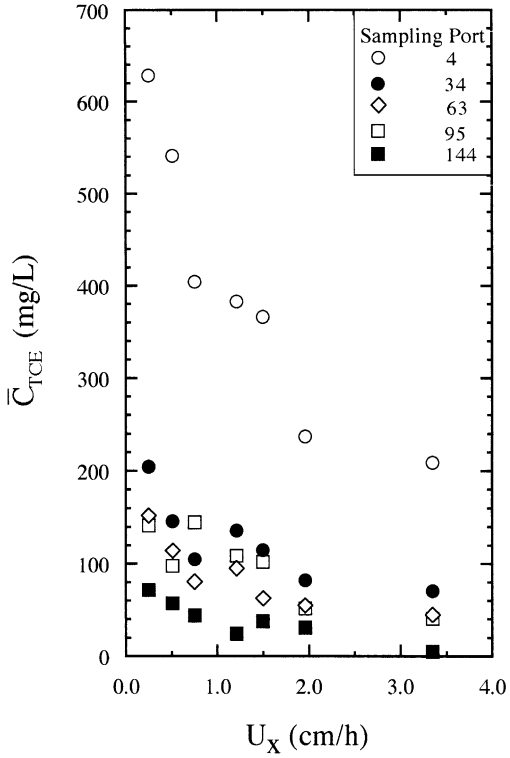

Fig. 2. Observed steady-state aqueous-phase TCE concentrations (average of the two values listed in Table 1) as a function of interstitial velocity at all five sampling ports.

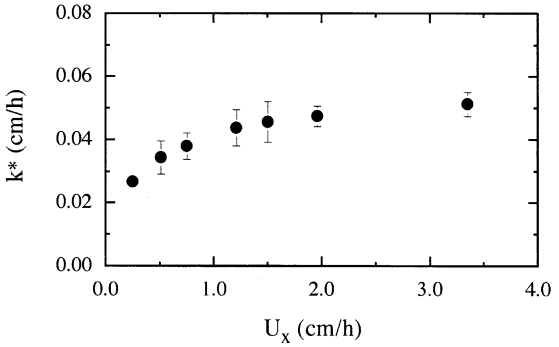

Fig. 3. Fitted time invariant overall mass transfer coefficients as a function of U_x evaluated from the averaged two sets of concentration measurements. Error bars represent the 95% confidence intervals.

analytical solution for a circular pool derived by [16] to the experimental data with the non-linear least squares regression program PEST [25]. Note that only k^* was fitted because all other required model parameters were independently determined.

The estimated time invariant mass transfer coefficients together with the corresponding 95% confidence intervals, as determined by PEST, are presented in Fig. 3. It should be noted that the k^* values in this figure are estimated from the average of the two mean aqueous-phase TCE concentrations obtained for each interstitial velocity. The plot indicates that k^* increases steadily with increasing U_x. It should be noted that as U_x continues to increase k^* approaches an asymptotic value. This trend has also been predicted by [15] and has been suggested by NAPL pool dissolution studies conducted by [12].

Fig. 4 shows the steady-state, aqueous-phase TCE concentrations observed at sampling locations 4, 34, and 144, along the centerline of the aquifer in the x–z plane together with the corresponding concentration contours predicted by the analytical solution using best-fit k^* values for $U_x = 0.51$, 1.21, 1.50, and 3.35 cm/h (experiments 4 through 7). It should be noted that the DNAPL pool is located between $-7.6 \leqslant x \leqslant 0$ cm (see Fig. 1). The solid circles represent sampling locations and the bold number next to each sampling location represents the corresponding average of the two observed aqueous-phase TCE concentrations obtained for each interstitial velocity. Fig. 4 shows relatively good agreement between the observed aqueous-phase TCE concentrations and the analytical solution. It is also shown in Fig. 4 that the vertical spreading of the dissolved TCE decreases with increasing interstitial velocity. Note that under the present experimental conditions the vertical spreading of the dissolved TCE is only a few centimeters thick.

Following procedures outlined by [15] a correlation relating the time invariant Sherwood number to overall Peclet numbers is proposed in the form

$$Sh^* = \alpha_1 (Pe_x^*)^{\alpha_2} (Pe_y^*)^{\alpha_3}, \tag{5}$$

where α_1, α_2, and α_3 are coefficients to be determined. The unknown correlation coefficients are evaluated by fitting the proposed correlation (5) to the seven experimentally determined k^* values presented in Fig. 3 by the nonlinear least squares regression program PEST [25]. The desired experimental, overall Sherwood number correlation is expressed as

$$Sh^* = 1.30 (Pe_x^*)^{0.12} (Pe_y^*)^{0.44}. \tag{6}$$

Fig. 5 compares the experimentally determined correlation (solid curve) with the experimentally determined Sh^* values (circles) and the [15] correlation (dashed curve) as a function of interstitial velocity. Note that predictions based on the numerically derived correlation (4) are higher than those predicted by the experimentally determined correlation (6) by approximately a factor of two. A possible explanation for the difference between the experimentally developed correlation (6) and the existing numerically determined correlation (4) can be

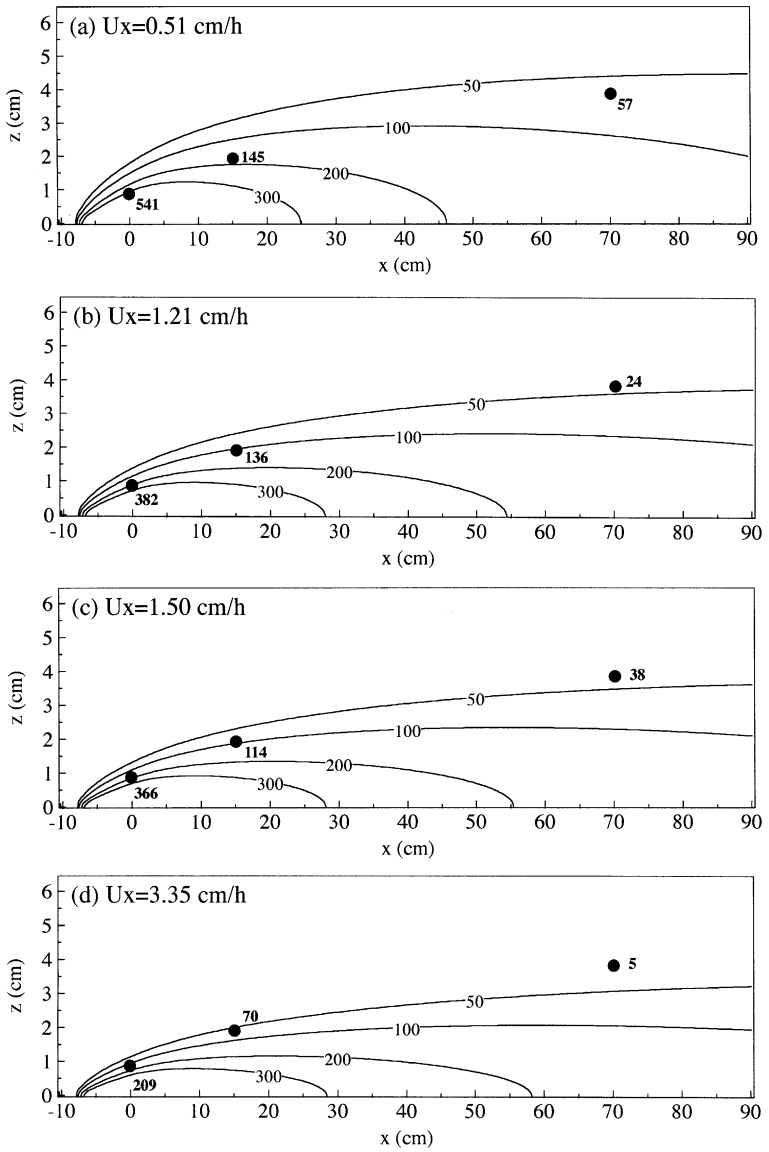

Fig. 4. Steady-state aqueous-phase TCE concentration contour plots in mg/L, down the centerline of the pool in the x–z plane, and observed concentrations at sampling locations indicated by the solid circles for (a) $U_x = 0.51$ cm/h, (b) $U_x = 1.21$ cm/h, (c) $U_x = 1.50$ cm/h, and (d) $U_x = 3.35$ cm/h.

attributed to the fact that the numerical correlation is based on numerically-generated data obtained from various elliptic pool shapes with longitudinal size ranging from 2.5 to 5 m, whereas the circular pool used in the present study is only 0.076 m in diameter. Note that a circular pool is just a special case of an elliptic pool with equal semiaxes. Chrysikopoulos [16] has shown that increasing the eccentricity of an elliptic pool, $\varepsilon = [1 - (b/a)^2]^{1/2}$ (where a, b are the major and minor semiaxes of an elliptic pool, respectively [L]), results to an increased overall Sherwood number.

6. Conclusions

Three-dimensional TCE pool dissolution experiments were conducted in a bench-scale model aquifer. A flat circular TCE pool with well-defined pool–water interfacial area was formed with the use of a specially designed base plate. Steady-state aqueous-phase TCE concentrations were collected at five locations within the experimental bench scale aquifer under seven different interstitial velocities. For each sampling set, a time invariant overall mass transfer coefficient was obtained

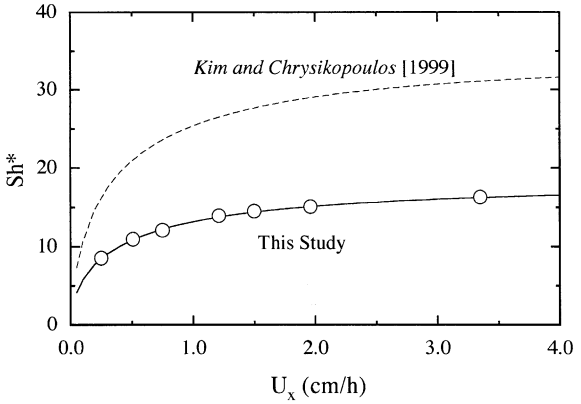

Fig. 5. Comparison between experimentally determined overall mass transfer correlation (6, solid curve) and the numerically determined correlation of [15] (4, dashed curve) as a function of U_x. The circles represent the experimentally determined *Sh** values.

by fitting the observed aqueous phase TCE concentrations with an existing analytical solution. An overall Sherwood number correlation based on seven experimentally determined mass transfer coefficients was developed. The additional four experiments presented in this work were essential for better determination of the correlation coefficients and extended the existing data set of mass transfer coefficients for TCE pool dissolution.

Acknowledgements

This research was sponsored by the Environmental Protection Agency, under Grant No. R-823579-01-0. Additional support from the University of California, Irvine for the purchase and maintenance of the constant temperature chamber is gratefully acknowledged.

References

[1] Anderson MR, Johnson RL, Pankow JF. Dissolution of dense chlorinated solvents into groundwater, 3, Modeling contaminant plumes from fingers and pools of solvent. Environ Sci Technol 1992;26(5):901–8.

[2] Lee KY, Chrysikopoulos CV. Numerical modeling of three-dimensional contaminant migration from dissolution of multicomponent NAPL pools in saturated porous media. Environ Geology 1995;26(3):157–65.

[3] Lee KY, Chrysikopoulos CV. NAPL pool dissolution in stratified and anisotropic porous formations. J Environ Eng, ASCE 1998;124(9):851–62.

[4] Holman H-YN, Javandel I. Evaluation of transient dissolution of slightly water-soluble compounds from a light nonaqueous phase liquid pool. Water Resour Res 1996;32(4):915–23.

[5] Mason AR, Kueper BH. Numerical simulation of surfactant-enhanced solubilization of pooled DNAPL. Environ Sci Technol 1996;30:3205–15.

[6] Jia C, Shing K, Yortsos YC. Advective mass transfer from stationary sources in porous media. Water Resour Res 1999;35(11):3239–51.

[7] Tatalovich ME, Lee KY, Chrysikopoulos CV. Modeling the transport of contaminants originating from the dissolution of DNAPL pools in aquifers in the presence of dissolved humic substances. Transp Porous Media 2000;38(1/2):93–115.

[8] Zhou D, Dillard LA, Blunt MJ. A physically based model of dissolution of nonaqueous phase liquids in the saturated zone. Transp Porous Media 2000;39: 227–55.

[9] Vogler ET, Chrysikopoulos CV. Dissolution of nonaqueous phase liquid pools in anisotropic aquifers. Stochastic Environmental Research and Risk Assessment 2001; 15:33–46.

[10] Schwille F. Dense chlorinated solvents in porous and fractured media, translated by J.F. Pankow. Chelsea, Michigan: Lewis Publishers, Inc., 1988, 146pp.

[11] Chrysikopoulos CV, Voudrias EA, Fyrillas MM. Modeling of contaminant transport resulting from dissolution of nonaqueous phase liquid pools in saturated porous media. Transp Porous Media 1994;16:125–45.

[12] Seagren EA, Rittmann BE, Valocchi AJ. An experimental investigation of NAPL pool dissolution enhancement by flushing. J Contam Hydrol 1999;37:111–37.

[13] Saba T, Illangasekare TH. Effect of groundwater flow dimensionality on mass transfer from entrapped nonaqueous phase liquid contaminants. Water Resour Res 2000; 36(4):971–9.

[14] Chrysikopoulos CV, Lee KY, Harmon TC. Dissolution of a well-defined trichloroethylene pool in saturated porous media: Experimental design and aquifer characterization. Water Resour Res 2000;36(7):1687–96.

[15] Kim T-J, Chrysikopoulos CV. Mass transfer correlations for nonaqueous phase liquid pool dissolution in saturated porous media. Water Resour Res 1999;35(2): 449–59.

[16] Chrysikopoulos CV. Three-dimensional analytical models of contaminant transport from nonaqueous phase liquid pool dissolution in saturated subsurface formations. Water Resour Res 1995;31(4):1137–45.

[17] Incropera FP, DeWitt DP. Fundamentals of heat and mass transfer. 3rd ed. New York: Wiley, 1990, 919pp.

[18] Chrysikopoulos CV, Lee KY. Contaminant transport resulting from multicomponent phase liquid pool dissolution in three-dimensional subsurface formations. J Contam Hydrol 1998;31(1–2):1–21.

[19] Khachikian C, Harmon TC. Nonaqueous phase liquid dissolution in porous media: Current state of knowledge and research needs. Transp Porous Media 2000;38(1/2): 3–28.

[20] Chrysikopoulos CV, Kim T-J. Local mass transfer correlations for nonaqueous phase liquid pool dissolution in saturated porous media. Transp Porous Media 2000; 38(1/2):167–87.

[21] de Marsily G. Quantitative hydrogeology, groundwater hydrology for engineers. San Diego, CA: Academic Press, 1986, 440pp.
[22] Hayduk W, Laudie H. Prediction of diffusion coefficients for nonelectrolytes in dilute aqueous solutions. AIChE Journal 1974;20(3):611–5.
[23] Chrysikopoulos CV. Artificial tracers for geothermal reservoir studies. Environ Geology 1993;22:60–70.
[24] Mackay D, Shiu WY, Ma KC. Illustrated handbook of physical-chemical properties and environmental fate for organic chemicals, Volatile organic chemicals, vol. 3. Chelsea, Michigan: Lewis Publishers, 1992, 916pp.
[25] Doherty J, Brebber L, Whyte P. PEST: Model-Independent Parameter Estimation. Brisbane, Australia: Watermark Computing, 1994.